Available online at www.sciencedirect.com
ScienceDirect
Marine Chemistry 109 (2008) 152–164
MARINE CHEMISTRY
www.elsevier.com/locate/marchem

Photochemical and biochemical controls on reactive oxygen and iron speciation in the pelagic surface ocean

Song-Miao Fan *

NOAA Geophysical Fluid Dynamics Laboratory, P.O. Box 308, 201 Forrestal Road, Princeton, NJ 08542, United States

Received 9 November 2007; received in revised form 17 January 2008
Available online 26 January 2008

Abstract

A time-dependent chemistry model is used to predict reactive oxygen species (ROS = $H_2O_2 + O_2^-$) and dissolved Fe (DFe) speciation in the surface ocean. A new feature of the model is inclusion of biological sources of superoxide. The model suggests that biochemistry mediated by phytoplankton cells is as important as photochemistry for the formation of ROS. Formation of stable organic Fe(III) complexes (FeL) maintains the concentration of DFe in seawater. Iron speciation in the model is also controlled by biochemical and photochemical processes, and is far from thermodynamic equilibrium. During light periods, photo-reduction of FeL produces dissolved inorganic iron much more than thermal decomposition and cell-surface reduction of FeL, thus facilitating phytoplankton uptake of iron in the ocean. During the nighttime, O_2^- produced by reductases on cell surfaces both reacts with FeL, producing Fe(II), and retards the oxidation of Fe(II) and subsequent formation of FeL; therefore significant levels of bio-available Fe is maintained through this period. Photo-reduction nearly balances the formation of FeL in the model, and may control bioavailability of dissolved iron. This suggests a possible extracellular mechanism of iron and light colimitation to primary productivity. A phytoplankton growth limitation by FeL photo-reduction depends on its rate coefficient for which we need extensive measurements in natural seawater.
Published by Elsevier B.V.

Keywords: Iron; Iron speciation; Iron and light colimitation; Hydrogen peroxide; Superoxide; Reactive oxygen; Kinetic model; Photodissociation; Photoreduction; Cell surface reductase

1. Introduction

Iron is an essential nutrient required for phytoplankton photosynthesis in the ocean (e.g., Morel and Price, 2003). Low concentrations of iron (frequently < 0.2 nM) are thus limiting primary productivity in many parts of the ocean (Martin, 1990). Furthermore, speciation of iron influences iron acquisition by marine organisms. In the Fe′ model of iron uptake by marine eukaryotic phytoplankton, inorganic dissolved Fe (often denoted by a prime) is acquired via binding of Fe(III)′ or Fe(II)′ to a surface ligand and subsequent internalization by transfer across the plasma membrane (Hudson and Morel, 1990, 1993; Sunda and Huntsman, 1995). However, the concentration of Fe′ is much lower than that of colloidal and chelated iron at thermodynamic equilibrium (e.g., Rue and Bruland, 1995; Wu and Luther, 1995; Kuma et al., 1996; Liu and Millero, 2002). Iron uptake mediated by siderophore or surface reductases has been observed in cultured media for certain phytoplankton species, which suggests an adjunctive ligand substitution mechanism (Stinzi et al.,

* Tel.: +1 609 452 6569.
E-mail address: Songmiao.Fan@noaa.gov.

0304-4203/$ - see front matter. Published by Elsevier B.V.
doi:10.1016/j.marchem.2008.01.005

2000; Wells and Trick, 2004) or uptake via a surface-bound Fe(II) intermediate (Shaked et al., 2005). A multi-copper oxidase and two iron permeases were identified in the diatom *Thalassiosira pseudonana* that together could deliver surface-bound Fe(II) (Armbrust et al., 2004), this mechanism should be particularly advantageous when Fe(II)′ is much more abundant than Fe(III)′ in seawater. The direct uptake of Fe-siderophore complexes is slow compared to that facilitated by surface reductases (Maldonado and Price, 1999, 2001).

In addition to the biochemical processes, photo-reduction of the iron colloids and complexes may lead to rapid formation of Fe′ and phytoplankton uptake in the surface ocean (e.g., Voelker et al., 1997; Barbeau et al., 2001; Borer et al., 2005; Barbeau, 2006). The influence of visible (VIS: 400–700 nm) light on FeL photo-reduction is comparable to that of ultraviolet A (UVA: 315–400 nm) and ultraviolet B (UVB: 280–315 nm) because it has the highest total energy and penetrates deepest into the ocean, while UVB has the highest quantum yield and the highest extinction coefficient (Rijkenberg et al., 2005). Similar spectral dependence was observed for the photo-reduction of colloids of iron oxides (e.g., Wells et al., 1991), and for the photochemical production of reactive oxygen (e.g., Gerringa et al., 2004). Therefore, photo-reduction and photochemical cycling of Fe can occur deep in the photic zone as well as near the surface.

The importance of FeL photo-reduction is indicated by the combination of two recent as well as previous studies (see below). In the first, a high correlation between dissolved Fe and ligand concentrations was observed in the Bering Sea, suggesting a significant role for FeL in the solubility and bioavailability of dissolved Fe (Buck and Bruland, 2007). The bioavailability of FeL has been shown by the observed decrease of [Fe]/[ligand] ratio as water is advected from inner to outer shelf domains in the Bering Sea, which indicates removal of Fe from the FeL complex via biological uptake. In the second, measurements show persistence of Fe(II) (~20−200 pM, 10–50% of total Fe) in surface waters of the western subarctic Pacific, which provides evidence for significant photochemical cycling of iron and its role in phytoplankton uptake of this nutrient (Roy et al., 2008). The high ratio of Fe(II)/Fe(III) is favorable to maintain a high concentration of dissolved inorganic iron and to prevent the formation and sinking of particulate iron.

A time-dependent chemistry model is developed in this study to investigate the influence of photochemical and biochemical processes on iron speciation in the surface ocean to assess the relative importance of various pathways for phytoplankton uptake of iron. Admittedly, the surface ocean is a complex system of interrelated biological, chemical, and physical processes. Processes not included in the model may be important in the subsurface layer, in the coastal ocean, in the sea ice zone, or for other reasons. Our goals in this study are to understand Fe speciation in a low-complexity model and to find out whether biochemical processes involving surface reductases have significant influence on Fe speciation. This study, by including biochemical processes, complements previous modeling studies that have only considered sunlight-mediated iron redox cycling (e.g., Miller et al., 1995; Rose and Waite, 2003a; Meunier et al., 2005; Weber et al., 2005; Tagliabue and Arrigo, 2006).

A description of the model is presented in Section 2. Model results and discussions are presented in Section 3, starting with the sources and sinks of ROS and followed by Fe chemistry. Discussions focus on the impact of biochemical O_2^- production as a new feature of the model. We compare biochemical and photochemical controls on Fe speciation, and compare the estimated rates of photo-reduction and biological reduction of FeL. Model results are also compared to previous studies to highlight differences and uncertainties. A summary of the main results are presented in Section 4 with suggestions for needed measurements and for model development.

2. Model description

The chemical and biochemical reactions included in the model are listed in Table 1. The rate (r) of a reaction is calculated as the product of the kinetic rate coefficient (k) and the concentrations of reactants ([A] and [B] in units of M or mol l^{-1}), $r = k[A][B]$, and is in a unit of M s^{-1}. For photo-dissociation reactions [A] is the number of photons absorbed (acting on B) in a unit volume of seawater. This rate counts as a loss for the reactants on the left-hand-side and a production for the species on the right-hand-side of each reaction shown in Table 1. The time derivative of each species in a box model (i.e., neglecting diffusion exchange with neighboring spaces) is then the sum of production rates minus the sum of loss rates for that species. Given initial concentrations for all species considered in the model, the set of equations written for the time derivatives are integrated forward in time to yield annually stationary, seasonally and diurnally time-dependent concentrations. The only cause of variation considered in the model simulations is solar irradiance.

The photo-dissociation rate coefficients are calculated following Weber et al. (2005), based on the number of photons absorbed in the visible and

Table 1
Aqueous-phase reaction rate constants

Reaction No.	Reaction	k $M^{(1-n)}$ s^{-1}	*n*	References/Notes
A01	$Fe(II)' + O_2 \rightarrow Fe(III)' + O_2^-$	10.	2	Millero et al. (1987)
A02	$Fe(II)' + H_2O_2 \rightarrow Fe(III)' + OH + OH^-$	7.2×10^4	2	Millero and Sotolongo (1989)
A03	$Fe(II)' + O_2^- \rightarrow Fe(III)' + H_2O_2$	1.0×10^7	2	Rush and Bielski (1985)
A04	$Fe(III)' + O_2^- \rightarrow Fe(II)' + O_2$	1.5×10^8	2	Rush and Bielski (1985)
A05	$Fe(III)' + Ligand \rightarrow FeL$	2.0×10^6	2	Witter et al. (2000)
A06	$Fe(III)'$ (+Colloid) $\rightarrow$ CFe	2.8×10^{-5}	1	Weber et al. (2005)
A07	CFe + Particle $\rightarrow$ PFe	14.	2	Weber et al. (2005)
A08	$Fe(III)' + Cell \rightarrow BFe$	0.	2	Net biological uptake set to zero
A09	$FeL \rightarrow Fe(III)' + Ligand$	1.0×10^{-6}	1	Witter et al. (2000)
A10	$Fe(III)' + h\nu \rightarrow Fe(II)' + OH$	1.5×10^{-5}	1	See footnote
A11	$FeL + h\nu \rightarrow Fe(II)' + Ligand$	1.0×10^{-3}	1	See footnote
A12	$CFe + h\nu \rightarrow Fe(II)'$	2.3×10^{-4}	1	See footnote
A13	$PFe + h\nu \rightarrow Fe(II)'$	2.3×10^{-4}	1	See footnote
A14	PFe $\rightarrow$ sinking loss	0.	1	Set to zero
A15	$FeL + O_2^- \rightarrow Fe(II)' + O_2$	1.5×10^5	2	Rose and Waite (2005)
A16	O_2 + Eukaryotes + $h\nu \rightarrow O_2^-$		1	See footnote and text
A17	CDOM + $h\nu \rightarrow O_2^-$	8.0×10^{-7}	1	See footnote and text
A18	$HO_2 + O_2^-$ (+ H^+) $\rightarrow H_2O_2 + O_2$	1.0×10^8	2	Bielski (1978)
A19	H_2O_2 (+ROM) $\rightarrow$ products	5.8×10^{-6}	1	Moore et al. (1993)
A20	$Cu(I) + O_2 \rightarrow Cu(II)' + O_2^-$	4.6×10^5	2	Bjergbakke et al. (1976)
A21	$Cu(I) + H_2O_2 \rightarrow Cu(II)' + OH + OH^-$	7.0×10^3	2	Berdnikov (1973)
A22	$Cu(I) + O_2^-$ (+$2H^+$) $\rightarrow Cu(II)' + H_2O_2$	9.4×10^9	2	Piechowski von et al. (1993)
A23	$Cu(II)' + O_2^- \rightarrow Cu(I) + O_2$	8.0×10^9	2	Rabani et al. (1973)

Footnotes: All photoreaction (A10–A13, A17) rate coefficients are given at 30 μmol photons m^{-3} s^{-1} (Weber et al., 2005). A16 is lumped into A17.

ultraviolet spectral bands. But the spectral dependence is not considered explicitly in the present model. The rate coefficients for photo-reduction of iron species (FeL, colloidal and particulate Fe) remain highly uncertain in the surface ocean. The measured rates of colloidal iron photo-reduction range from 1.4×10^{-6} to 2.3×10^{-4} s^{-1} under conditions of natural light near noontime (Waite and Morel, 1984; Wells and Mayer, 1991; Johnson et al., 1994; Barbeau and Moffett, 2000). The significant differences are caused by differences in the reactivity of the iron colloids, the presence of electron donors (e.g., fulvic acid and oxalate), and detection methods (Sulzberger and Laubscher, 1995; Voelker et al., 1997; Barbeau and Moffett, 2000; Borer et al., 2005). Similarly, the measured photoreduction rates of organic iron complexes vary significantly, with noontime rates ranging from 1.7×10^{-4} to 1.3×10^{-3} s^{-1} depending on the chemical structure of ligands present in seawater (Kuma et al., 1992; Emmenegger et al., 2001; Barbeau et al., 2001, 2003; Rijkenberg et al., 2006). Redox iron cycling also occurs through biotic uptake, grazing and remineralization processes (e.g., Barbeau et al., 1996), but is relatively slow and thus neglected in the present model.

The rate coefficients for FeL formation (A05 in Table 1) and thermal decomposition (A09) have been measured for various natural organic matters (Witter and Luther, 1998; Witter et al., 2000; Rose and Waite, 2003b). For instance, in the Northwestern Atlantic Ocean, formation rate constants (k_f) of FeL from inorganic Fe(III)′ and organic ligands ranged from 4.2×10^4 to 1.1×10^6 M^{-1} s^{-1} and dissociation rate constants (k_d) from 1.0×10^{-7} to 3.9×10^{-5} s^{-1} while the stability constants of the FeL complexes were nearly invariant ($\log K_{Fe'L}$ = 12.2±0.5 at 500 m to 12.9±0.3 at 200 m depth). We use two pairs of rate constants ($k_f=2\times10^6$ M^{-1} s^{-1} and $k_d=1\times10^{-6}$ s^{-1} versus $k_f=2\times10^5$ M^{-1} s^{-1} and $k_d=1\times10^{-7}$ s^{-1} with the same stability constant) in our simulations to account for the uncertainties.

The total source of O_2^- is constrained by measurements of H_2O_2 in seawater, but has a variety of pathways. The primary source of O_2^- in the surface ocean is specified to depend on the photolysis of colored dissolved organic matter (CDOM) and cell surface O_2 reduction. Other sources, including photolysis of nitrate and nitrite are lumped into the production from CDOM photolysis for their common light dependence. Cell surface production of O_2^- is induced by cellular respiration through "leakage" of electrons from the respiration chain and their reduction of molecular oxygen (Marshall et al., 2005), and is partially controlled by electrons donated through photosynthetic electron transfer (Marshall et al., 2002). While the direct enzymatic production of O_2^- by surface reductases seems probable, a metabolite released into

seawater may also reduce O_2 to O_2^- (Kustka et al., 2005). The cellular respiration-induced enzymatic O_2 reduction is assumed to be constant over a diel cycle but varying with daily mean irradiance over an annual cycle to account approximately for the seasonal variation of biomass. The dismutation of O_2^- produces H_2O_2, which is catalyzed by Cu and Fe ions. We discuss the relative contribution of these O_2^- sources in Section 3.

Specified chemical concentrations and model parameters are listed in Table 2. In this study, we specify the total dissolved Fe concentration (0.1 nM), which includes colloidal and particulate iron that is photolabile, and the total concentration of organic ligands (1.8 nM). Depending on the concentration of ligands, colloidal and particulate Fe may be comparable to or higher than truly dissolved Fe concentrations (e.g., Wu et al., 2001; Nishioka et al., 2001, 2003, Takata et al., 2006). In the tropical Atlantic Ocean, soluble Fe is relatively constant (0.2−0.4 nM) while colloidal and particulate Fe vary spatially and temporally with atmospheric deposition of desert dust aerosols (Bergquist et al., 2007). Our main conclusions do not depend on the concentration of iron (Section 3). Our model simulations are restricted to conditions with ligands in permanent excess of dissolved iron concentration (Buck and Bruland, 2007). The concentration of CDOM is specified in the model to predict observed H_2O_2 concentrations. The concentration of reactive organic matter (ROM) that reacts with H_2O_2 is specified to balance the production of H_2O_2 from O_2^- so as to give the observed diurnal cycle of H_2O_2 in the surface ocean.

The chemistry in this model is non-linear, particularly for the dismutation of O_2^-, as a result, the model results are sensitive to the averaging depth. We chose to model photochemistry in the top 30 m of the surface ocean where 50−80% of the biological productivity and photochemistry occur depending on the light extinction coefficient (0.04 −0.08 m^{-1} in the visible spectrum) and mixing is relatively fast (diffusivity = 10^{-4} to 10^{-3} m^2 s^{-1}). The solar irradiance is calculated based on the empirical formula of Lumb (1964), which is sufficiently accurate for our purpose (Frouin et al., 1989). The effect of cloud cover is neglected.

Table 2
Parameters used in the standard model

Parameter	Value	Note
Ligand (nM)	1.8	For iron(III) complexation
Particle (g L^{-1})	0.1	For colloidal Fe adsorption
Dissolved O_2 (μM)	240	
CDOM (μM)	3.0	Colored dissolved organic matter
ROM (nM)	10.	Organic matter reacting with H_2O_2
Dissolved Fe (nM)	0.1	
Free Cu ion (pM)	2.0	
pH	8.1	

This study focuses on the budget of reactive oxygen and diel cycles of dissolved Fe species driven by photochemistry. Dust deposition, biological uptake, sinking of particulate Fe and vertical mixing are not included in the present model simulations. These processes are important controls on the total Fe concentration, but have only small influence on the diel cycle of Fe speciation. However, we discuss model sensitivities to dissolved Fe and Cu concentrations, biological sources of ROS, and photo-dissociation rate coefficient of FeL. These parameters are related directly or indirectly to dust deposition, biological productivity, sinking of particulate Fe, and mixed layer depth. Our main conclusions are not dependent on whether these processes are fully represented in the model.

3. Results and discussions

3.1. Reactive oxygen budget

Sensitivity studies reveal the utility of measurements of H_2O_2 concentration as a constraint on photochemistry in the surface ocean. Fig. 1a shows the two specifications of primary O_2^- production rate, with and without the biochemical source, respectively. The two specifications have the same total production integrated over a 24-hour period, but different diel cycles and amplitudes. The nighttime concentrations of O_2^- are maintained by biochemical source alone, which could be significant relative to daytime concentrations (Fig. 1b). To our knowledge, however, there are no measurements of O_2^- in seawater to corroborate the model result.

Fig. 1c shows the diel cycles of H_2O_2 with and without biochemical O_2^- production. The amplitude is about 20 nM with only photochemical source of O_2^- specified in the model, and is about 10 nM with a nighttime O_2^- source but the same total daily production (see Fig. 1a). A diel cycle amplitude of 20–30 nM has been observed in tropical to subtropical oceans (Palenik and Morel, 1988; Yuan and Shiller, 2001, 2005). However, a diel amplitude of H_2O_2 over 40 nM was observed at the Bermuda Time Series Station (BATS, 32°N) in March, likely due to increased biological productivity during the spring bloom (Avery et al., 2005). It is noted that a lifetime (e-folding time) of 2 days is specified in the model to give a loss of H_2O_2 against reaction with organic matter (A19 in Table 1). Dark reaction was observed to destroy H_2O_2 in times as short as <1 day in highly productive coastal oceans to >5 days in oligotrophic oceans (Moore et al.,

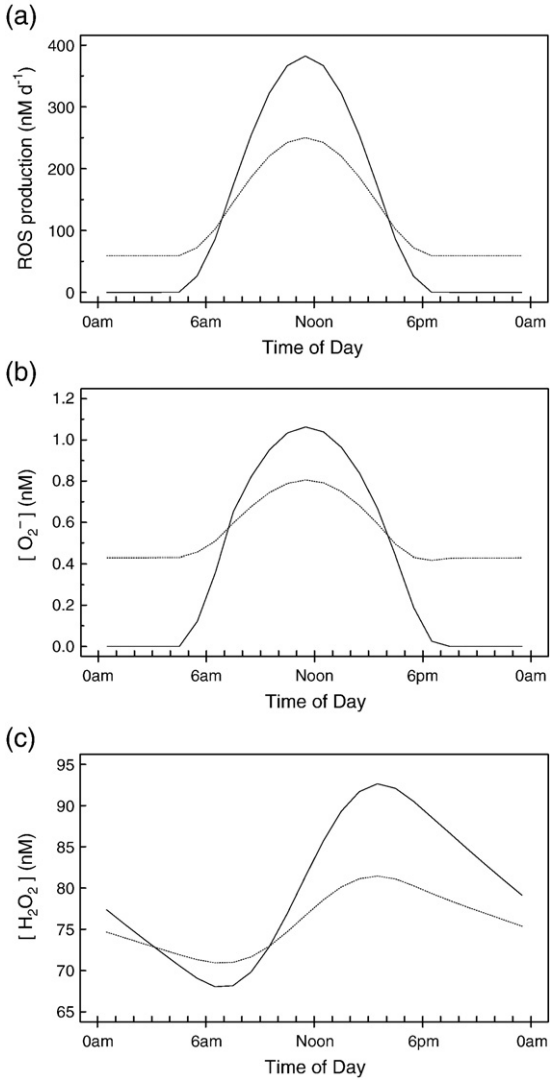

Fig. 1. (a) Prescribed rates for reactive oxygen species (ROS) production, (b) concentrations of O_2^- radical, (c) concentrations of H_2O_2, averaged annually by time of day. Dotted lines indicate model simulation with a biochemical source of ROS, and solid lines indicate simulation without a biochemical source (standard model).

1993; Yuan and Shiller, 2001, 2005; Avery et al., 2005). The large variability in the observed decay rates is likely caused by variations in dark production of H_2O_2 (Palenik and Morel, 1988) as well as peroxidase and catalase concentrations on plasma membranes and dissolved in seawater. These enzymes are produced by most marine organisms and have been suggested to be responsible for most H_2O_2 decomposition in coastal seawater (Moffet and Zafiriou, 1990).

Fig. 2 shows the seasonal cycle of H_2O_2 at the BATS location, where a surface concentration of approximately 40 nM in March and 80 nM in August have been

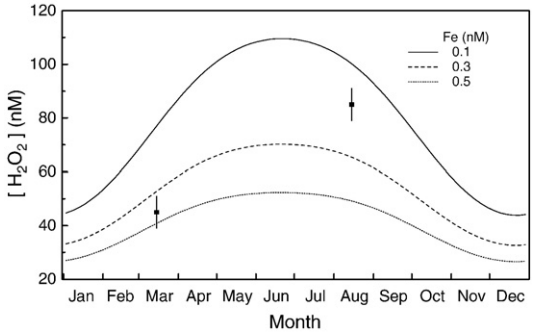

Fig. 2. Daily mean concentrations of H_2O_2 in surface seawater at 32° N in the standard model. Dissolved Fe is specified to be 0.1, 0.3 and 0.5 nM, respectively. Symbols show measurements of Avery et al. (2005).

observed (Avery et al., 2005). The concentrations are higher in the summer and lower in the winter, following the trend in production of superoxide. The concentration of H_2O_2 decreases with increased concentrations of dissolved Fe (Fig. 2), a relationship observed in the Southern Ocean during an iron enrichment experiment (Croot et al., 2005). This may be explained by a budget analysis of the reactive oxygen species (Fig. 3). Ferric ions react with O_2^- to form O_2 and Fe(II) (A04), more rapidly than the reverse reaction (A01), causing a loss of reactive oxygen. The soluble Fe observed near Bermuda is about 0.1 nM (Wu et al., 2001), but higher concentrations may result from (1) episodic eolian iron input which at this location is most pronounced in the summer (Sedwick et al., 2005; Bergquist et al., 2007), and (2) upwelling of water from below the mixed layer which is most significant in the winter. With iron deposition during the passage of a dust plume, an increase of dissolved Fe from 0.1 nM to 0.5 nM may decrease H_2O_2 from 100 nM to 50 nM in the Sargasso Sea in August (Fig. 2). In contrast, the concentration of H_2O_2 is not sensitive to dissolved inorganic Cu in the model

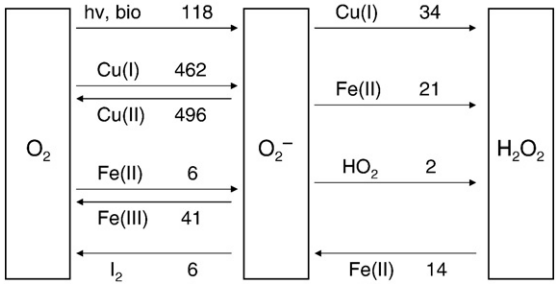

Fig. 3. Annual average rates (units: nM d^{-1}) of reactions leading to the formation and loss of superoxide in the standard model. Arrows point from reactants to products indicated in boxes. Second reactants and rates are indicated above or below the arrows.

(results not shown). As shown in Fig. 3, reactions with Cu ions cause about equal conversions of O_2^- to O_2 (A23−A20) and O_2^- to H_2O_2 (A22).

An annual average budget for H_2O_2 is calculated based on the standard model simulation and is shown in Table 3. The dismutation reactions of O_2^- involving Fe(II) and Cu(I) ions are mainly responsible for the formation, while reactions with the Fe(II) ion and organic matter constitute the main loss of H_2O_2 in this model. The total production and loss is 56 nM d^{-1}, which corresponds to a production of O_2^- at 118 nM d^{-1} by CDOM photolysis and cell surface reduction of oxygen. The photochemical source of O_2^- is only about 30 nM d^{-1} in oligotrophic ocean water, estimated based on an extrapolation of surface measurements to 30 m depth using a light extinction coefficient of 0.15 m^{-1} for the ultraviolet wavelengths (Mopper and Zhou, 1990; Micinski et al., 1993; Moore et al., 1993; Gerringa et al., 2004). The biochemical source of O_2^- must account for the remainder (88 nM d^{-1}) and is nearly 3-fold greater than the photochemical source.

Previously, extracelluar O_2^- production was measured at ~ 8.4×10^{-16} mol $cell^{-1}$ h^{-1} in *Thalassiosira weissflogii* (a marine diatom species) cultures (Kustka et al., 2005). Electron transport across the plasma membrane has been associated with a variety of fundamental physiological processes, including proton excretion and nutrient acquisition. Superoxide production in the raphidophyte *Chattonella* species, which are common in red tides, is up to 100-fold greater than in most other algae, followed by the dinoflagellate species (Marshall et al., 2005). Hydrogen peroxide production by a marine phytoplankter (*Hymenomonas carterae*, coccolithophorid species) was measured to be $1-2\times10^{-14}$ mol $cell^{-1}$ h^{-1} (Palenik et al., 1987). If we use the O_2^- production rate measured in *T. weissflogii* cultures for a eukaryotic phytoplankton population of 4×10^6 cells L^{-1} (DuRand et al., 2001), the biological production of O_2^- would be 81 nM d^{-1}. Similarly, if 10^4 coccolithophorid cells L^{-1} (DuRand et al., 2001) produced H_2O_2 at the rate measured for *H. caterae*, their total contribution would be 2.4 −4.8 nM d^{-1} which is equivalent to 5−10 nM d^{-1} for O_2^- production. Although production of H_2O_2 may not be a general characteristic of coccolithophorids (Palenik and Morel, 1988). The populations of *Prochlorococcus* and *Synechococcus* are on the order of 10^7 cells L^{-1} in waters near Bermuda, but we do not have measurements of O_2^- production for these species whose cell surface area is on the order of 100-fold smaller than *T. weissflogii*.

In bottle incubations of samples taken from a depth of 40 m in the Sargasso Sea, net dark decomposition of H_2O_2 occurred in some surface samples, but on average, net dark production of H_2O_2 was observed, at 1−3 nM h^{-1} (Palenik and Morel, 1988). The organisms and mechanisms responsible for the dark production remain unknown. Both respiratory and photosynthetically derived reductants may act as cytosolic electron donors for the plasma membrane reductase (Davey et al., 2003). Dark decay experiments show that filtration of seawater samples significantly increases the half-life of H_2O_2 (Cooper et al., 1989; Moore et al., 1993). This was suggested to confirm the role of phytoplankton cells in H_2O_2 destruction. Whether phytoplankton cells cause a source or a sink for H_2O_2 likely depends on the species and its growth environment. Because we do not have an observational constraint to estimate H_2O_2 production and decay activities in the dark separately, only a net decay rate coefficient can be estimated based on measurements.

The photochemical source of O_2^- depends on concentration of CDOM which is specified to be 3 μM corresponding to a photo-dissociation frequency of 8×10^{-7} s^{-1} assumed in the standard model and 2×10^{-7} s^{-1} in the model with a biochemical source of O_2^- (at 30 μmol m^{-3} s^{-1} absorbed photons). The real concentration of CDOM molecules could be 10 to 100-fold lower and their photo-dissociation frequency 10 to 100-fold higher than assumed. The lifetime of CDOM

Table 3
Annual average rates of superoxide production in the surface ocean (0–30 m)

Source of reactive oxygen	Rate nM h^{-1}	Rate nM d^{-1}	Note/Reference
Model H_2O_2 source	2.3	56	
Model O_2^- source	4.9	118	
Estimated photochemical O_2^- production[a]	1.4	34	Micinski et al. (1993)
Estimated photochemical OH production[a]	1.3	30	Mopper and Zhou (1990)
Missing O_2^- source	3.7	88	Model − photochemical
Estimated eukaryotic phytoplankton O_2^- production at 4×10^6 cells L^{-1}	3.4	81	Kustka et al. (2005)
Estimated cocolith H_2O_2 production × 2 at 1×10^4 cells L^{-1}	0.3	7	Palenik et al. (1987)

[a] Daytime near surface measurements in the open ocean scaled to 24-hour average light intensity in the 0–30 m water column using an extinction coefficient of 0.15 m^{-1} for UV.

has been estimated to be about 100 days against photo-oxidation in the Sargasso Sea under stratified conditions (Nelson et al., 1998). This, combined with the estimated 30 nM d^{-1} photochemical O_2^- production, suggests that the concentration of CDOM is about 3 μM in the surface water of Sargasso Sea, assuming photolysis of each CDOM molecule yields one O_2^- molecule. However, we do not know how many O_2^- molecules can be produced by each CDOM molecule and a series of daughter molecules. The concentration of CDOM has been measured in terms of light extinction and fluorescence, but not in moles per unit volume. The concentration of CDOM was estimated to be about 10 μM C and the total dissolved organic carbon (DOC) about 50 μM C in the Middle Atlantic Bight influenced by terrestrial inputs (Vodacek et al., 1997), a smaller fraction of the total DOC is expected to be colored in the remote ocean. Measurements of CDOM show distinct seasonal cycles in abundance and distribution that are not directly related to dissolved matter concentration, primary productivity or phytoplankton standing stock, and that transformations from CDOM to DOM and *vice versa* may take place with little change in carbon content (Nelson et al., 1998). Upwelling of deep water provides a source of CDOM, but new production of CDOM by microbes is also important which leads to net CDOM production during spring and summer and net destruction in fall in surface layers of the Sargasso Sea (Nelson et al., 2004).

3.2. Iron speciation and cycling

Fig. 4 shows the annual average diel cycles of Fe(II), Fe(III), and FeL at 32°N (the latitude of Bermuda) for the simulations with a biochemical source of O_2^- at night. At the high rate of FeL photolysis (Fig. 4a), Fe(II) increases rapidly from 5:00 am to 8:00 am local time to become the dominant species (~ 70% of DFe), and remains stable with a broad peak between 8 am and 4 pm, then decreases rapidly from 4 pm to 6 pm to ~ 10% DFe concentrations. The diurnal cycle of Fe(III) follows that of Fe(II), but with only 1/6 the magnitude. Over 80% dissolved Fe is present in the form of FeL during the nighttime, and as low as 20% in the day, for the specified excess ligand concentration. When the photolysis rate is reduced by a factor of 10, FeL would remain to be the dominant species even during the midday hours (~ 60%, Fig. 4b). The concentrations of photo-labile colloidal and particulate Fe are low (<5% of total iron), and are neglected in Fig. 4. Formation of FeL and photo-dissociation of new particulate Fe together have effectively suppressed the sinking of particulate Fe by slowing its formation and preventing its metamorphosis into a more stable form and aggregation. As a result, the dissolved Fe concentration may be maintained, sometimes in large excess over the solubility limit of mineral iron (hydr)oxides, for biological uptake in the surface ocean.

Our model results of Fe speciation are similar to obtained by Weber et al. (2005) with permanent excess of organic ligands ([L] ≈ 1.5 nM) over dissolved iron concentrations: Fe(II)′ dominates Fe(III)′ as the readily bio-available species; FeL dominates photo-labile colloidal and particulate Fe as the less bio-available species. However, their model predicts zero Fe′ concentration during the nighttime because it does not have a biochemical source for ROS. Fig. 5 compares the diel cycles of [Fe′] (=[Fe(II)′]+[Fe(III)′]) calculated without a biochemical source of O_2^- in the dark (line A) and with the dark source (lines B and C). Significant levels of Fe′ are maintained through the dark hours when a biochemical source of O_2^- is present. First, O_2^- reacts with FeL to produce Fe(II)′ (A15 in Table 1). Secondly, because O_2^- reacts with Fe(III)′ 15-times faster than it with Fe(II)′, [Fe(II)′] is several times higher than [Fe(III)′] (see Fig. 4) when [O_2^-] is high

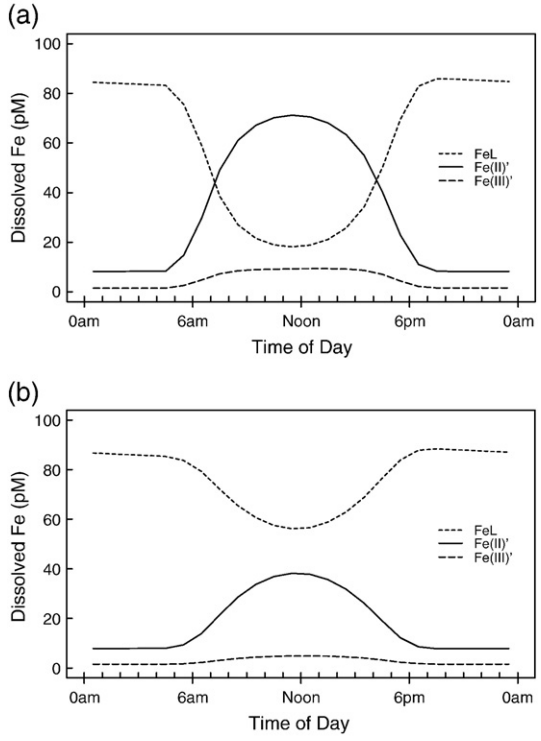

Fig. 4. Annual average diel cycles of dissolved Fe species, calculated with a biochemical source of ROS and with $k_{A11} = 1 \times 10^{-3}$ s^{-1} (a) and $k_{A11} = 1 \times 10^{-4}$ s^{-1} (b), respectively.

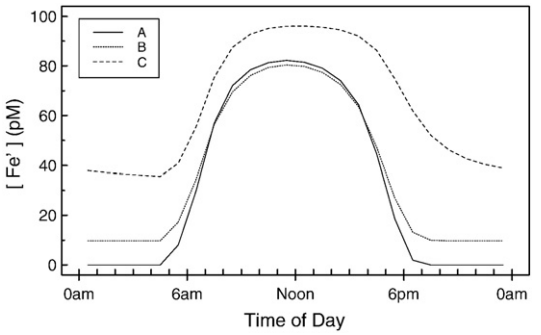

Fig. 5. Annual average diel cycles of inorganic Fe concentrations. Line A indicates standard model that has zero ROS source at night. Lines B and C indicate model simulations with a biochemical source of ROS at night. FeL formation and dissociation rate constants are both 10-fold slower in C than in A and B (see text).

enough to offset the oxidation of Fe(II)′ by O_2 and H_2O_2 so that the formation of FeL, colloidal and particulate Fe is kept slow. Slower formation of FeL with decreasing k_f also helps sustain a higher [Fe′] at night (compare lines B and C in Fig. 5).

The rates of cycling among iron species calculated in our model are significantly different from that of Weber et al. (2005). Fig. 6a and b show the iron cycling rates calculated for two FeL photo-dissociation rates (k_{A11} = 1×10^{-3} and 1×10^{-4} s^{-1}) respectively. Iron cycling from and to colloidal and particulate Fe is not important in our model and is neglected in Fig. 6a and b. Photo-dissociation of FeL is more important than its thermal decomposition in our model, while the opposite is true in Weber et al. (2005) due to a much larger value for k_d in their model. The reaction of FeL+O_2^- (A15) is also important in our model, which is not considered in Weber et al. (2005). The rates of Fe(II)′ and Fe(III)′ cycling are slower in our model due to the lower [Fe′] (noontime concentration ≈0.07 nM in the case of Fig. 6a and 0.04 nM in the case of Fig. 6b, compared to 0.35 nM in Weber et al. (2005)).

It is noted that the rates shown in Fig. 6a and b are linearly proportional to total iron concentration in the model, an increase of Fe by a factor of 5 would cause approximately 5-fold increases in the iron cycling rates. However, this would not be true if formation of stable particulate Fe is significant. Particulate Fe becomes increasingly less photolabile and less soluble with aging (e.g., Wu et al., 2001; Liu and Millero, 2002; Fujii et al., 2006). We specify in the model a low DFe in part to circumvent uncertainties related to the solubility of ferric oxyhydroxide and the formation and sinking of particulate iron. A low DFe is also in better agreement with observations in the surface ocean near Bermuda and in other regions of the world, some of which separate colloidal fraction (0.02–0.4 μm) from soluble fraction (<0.02 μm) (e.g., Wu et al., 2001; Boyd et al., 2005; Takata et al., 2006; Bergquist et al., 2007; Johnson et al., 2007). Dissolved Fe in the model simulations is mainly (>95%) in the soluble fraction.

The different rates shown in Fig. 6a and b indicate considerable compensation by all processes when k_{A11} is lowered by a factor of 10. For instance, the rate of A15 has increased from 0.13 to 0.33 nM d^{-1} as the rate of A11 has decreased from 1.12 to 0.28 nM d^{-1}, while the formation of FeL has decreased by only a factor of 2. For the typical range of ligand measurements (1−5 nM) (e.g., Rue and Bruland, 1995; Witter and Luther, 1998; Buck and Bruland, 2007), which is in permanent excess over dissolved Fe concentrations, iron speciation is dependent on but is not sensitive to [L]. However, the iron cycling rates are more sensitive to [L]. For example, annual average [FeL] increases from 0.065−0.072 nM while formation of FeL (A05) increases from 1.25−1.95 nM d^{-1} when [L] increases from 1.8−3.6 nM with other parameters unchanged from the standard simulation.

The speciation of dissolved Fe is also influenced by the dissolved inorganic Cu concentration, which is

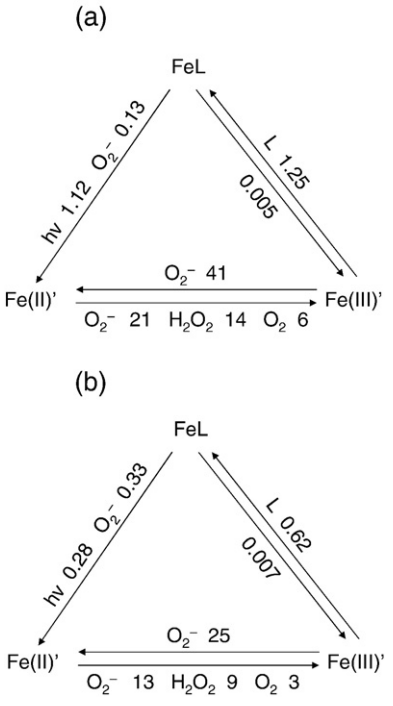

Fig. 6. Annual average rates of dissolved Fe cycling. Lines with arrow point from reactant to product, with the second reactant followed by corresponding rate (unit: nM d^{-1}) indicated next to each line. The rates are calculated with $k_{A11}=1\times10^{-3}$ s^{-1} (a) and $k_{A11}=1\times10^{-4}$ s^{-1} (b), respectively, and other parameters in the standard model.

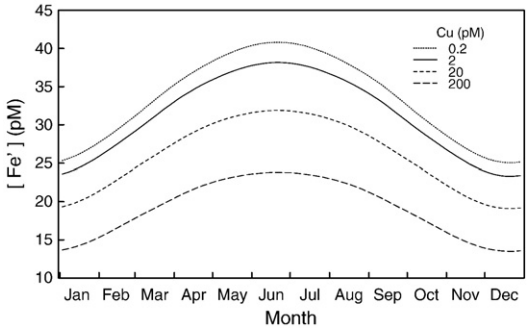

Fig. 7. Daily mean concentrations of total dissolved inorganic Fe (Fe(II)+Fe(III)) simulated for a range of free Cu ion concentrations: 0.2, 2, 20 and 200 pM. Other parameters are same as in the standard model.

specified in the model (Fig. 7), as discussed previously by Weber et al. (2005). The Cu^{2+} ion reacts rapidly with O_2^-, about 50-fold faster than Fe(III) does (Table 1). Increasing Cu^{2+} leads to lower O_2^- which leads to higher Fe(III) and more rapid formation of FeL. The net result of increasing Cu^{2+} is to decrease the sum of Fe(II)+Fe(III) even as Fe(III) is increased. Copper is efficiently complexed in seawater (Coale and Bruland, 1990); free Cu^{2+} concentrations are generally below 1 pM even though total Cu concentrations can be 1–2 nM in the open ocean (Moffet, 1995; Moffet and Dupont, 2007). Photochemical oxidation of copper complexing ligands occurs in the surface ocean (Laglera and van den Berg, 2006), causing the ligand concentrations to fall below total Cu as observed in the stratified Sargasso Sea (Moffet, 1995) and free Cu^{2+} concentrations in the range of 2–6 pM, higher enough to be toxic to some cyanobacteria (Mann et al., 2002). It is not known how fast $Cu(OH)_2(aq)$ can react with O_2^-, which is the dominant form of inorganic Cu in seawater ($[Cu(OH)_2(aq)]/[Cu^{2+}] \approx 150$ at pH=8). Deposition of mineral dust can increase the concentration of Cu^{2+} in the shallow mixed layer, which occurs frequently in the Sargasso Sea during the summer (Sedwick et al., 2005). Deep mixing tends to increase the concentration of copper complexing ligands in the mixed layer, lowering Cu^{2+} concentrations to ~0.1 pM (Moffet, 1995). Copper induced variability in dissolved inorganic Fe may be as large as the seasonal variation in the tropical Atlantic Ocean, but small in other ocean waters where Cu is low.

The model was also applied to iron chemistry in coastal seawater near Okinawa Island where measurements of H_2O_2, Fe(II) and total Fe were made in seawater samples filtered through a 0.45 μm filter (Arakaki et al., 2005). When the model is constrained with measurements of H_2O_2 it is able to predict the diel cycles of Fe speciation (results not shown). For instance, Fe(II) accounts for up to 70% of the total DFe in the day and 20%–30% at night. The main parameter is again the primary source of superoxide which is much higher in coastal waters than in the open ocean (Petasne and Zika, 1987; Mopper and Zhou, 1990; Micinski et al., 1993).

3.3. Photo-reduction versus biological reduction of FeL

The uptake of Fe by eukaryotic phytoplankton is primarily through Fe transporters at the cell surface that react with inorganic Fe species (Hudson and Morel, 1990; Sunda and Huntsman, 1995). At 32° N for a total dissolved Fe concentration of 0.1 nM, production of inorganic Fe from FeL photo-dissociation ranges from 0.8 nM d^{-1} in January to 1.5 nM d^{-1} in June in the standard model, and from 0.2–0.5 nM d^{-1} when the photo-dissociation rate coefficient is reduced by a factor of 10 (Fig. 8). The seasonal variability is larger at higher latitudes, for instance, from 0.5–1.7 nM d^{-1} at 50°N and from 0.2–1.8 nM d^{-1} at 60° N in the standard model, due to greater amplitude of solar irradiance (results not shown). Inorganic Fe may also be supplied by biological reduction of Fe(III) bound to organic ligands, which occurs through uptake of ferric siderophore complexes by heterotrophic bacteria (Armstrong et al., 2004) followed by microzooplankton grazing (Hutchins et al., 1993) or through an extracellular reduction step mediated by a cell surface reductase (Maldonado and Price, 2001; Shaked et al., 2005). Biological reduction was estimated to be in the range of 0.7–6.8 pM d^{-1} for a dissolved Fe of 0.07 nM (or 1–10 pM d^{-1} for a dissolved Fe of 0.1 nM as specified in our model) in the subarctic Pacific, compared to a steady-state Fe uptake of 2.4–24 pM d^{-1} by phytoplankton in situ (Maldonado and Price, 1999). The rates of FeL photo-dissociation calculated in our model

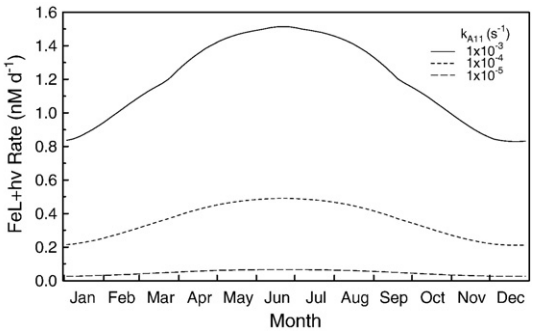

Fig. 8. Daily mean rates of FeL photoreduction simulated with three different rate coefficients ($k_{A11}=10^{-3}$, 10^{-4}, 10^{-5} s^{-1}) and other parameters in the standard model.

are much faster than that of the biological reduction. This is consistent with the observations that light enhanced the rates of Fe uptake by 15-fold, on average, for all size fractions of phytoplankton in the incubated subantarctic seawaters (Maldonado et al., 2005). If biological reduction were promoted by trans-membrane electron transport during photosynthesis, it would appear as photo-reduction in our study. However, the estimated rates of FeL reduction on cell surfaces have been shown to be small compared to that of photochemical reduction. While these estimates were based on the rates of phytoplankton uptake of Fe in measurements (Maldonado and Price, 1999; Shaked et al., 2005), it is possible that biochemical reduction of FeL is much faster but is offset by re-oxidation before phytoplankton uptake.

In conclusion, both measurements and model results confirm that formation of FeL and its photoreduction play an important role in the solubility and bioavailability of iron. Formation of FeL is balanced by photoreduction and reaction with superoxide in the model (see Fig. 6). Photochemical production of Fe(II) increases [Fe′] and enhances iron bioavailability significantly over biological reduction of FeL. It is further suggested that phytoplankton growth depends on photoreduction of FeL, which is a possible extracellular mechanism for iron and light colimitation for primary productivity under low Fe and low light conditions. This is in addition to the colimitation of phytoplankton growth by cellular Fe and photosynthetically active radiation (PAR) through photosynthesis (e.g., Armstrong, 1999; Boyd et al., 2001). A phytoplankton demands an increase of cellular Fe quota at a decreased solar irradiance in order to maintain the rates of N uptake and photosynthesis (Armstrong, 1999). Iron/PAR colimitation results when a phytoplankton fails to meet the requirement at low Fe concentrations, which occurs frequently for cells with a small surface-to-volume ratio (e.g., large centric diatoms).

4. Summary

A time-dependent chemistry model has been developed to study the budget of reactive oxygen and speciation of iron in seawater of the surface ocean. Measurements of H_2O_2 provide a useful constraint on seawater chemistry, including the rate of O_2^- production and Fe speciation. Model results suggest that biochemical sources and sinks of H_2O_2 are likely more important than photochemical processes in the oligotrophic ocean. By contrast, biological reduction of FeL is likely less important than photochemical reduction as a source of inorganic Fe and its subsequent uptake by phytoplankton. Biochemical and photochemical processes together drive iron speciation far from thermodynamic equilibrium and maintain a high inorganic fraction of total dissolved Fe, facilitating phytoplankton uptake of Fe in the ocean. Photochemical reduction converts FeL and colloidal/particulate Fe to dissolved inorganic Fe during sunlit hours while a high level of Fe′ is maintained at night by O_2^- from biochemical reduction of O_2 on phytoplankton cell surfaces. It is suggested that photoreduction of FeL may be a cause of iron and light colimitation of primary productivity under low Fe and low light conditions, in addition to the observed colimitation by Fe and PAR.

Some measurements are particularly needed to validate the chemistry model. These include concentration and production of O_2^- and H_2O_2 in both daytime and nighttime, at various depths, and for a range of phytoplankton species and population density. These measurements will reveal the importance of biological source of ROS as well as the dependence of ROS on CDOM concentration and solar irradiance. Concurrent measurements of various forms of iron in the surface ocean, including Fe(II)′ over diel and annual cycles, will provide quantitative information on the processes that influence iron chemistry. Seasonal measurements of organic ligands and FeL stability, including its formation and decomposition rate coefficients, are also needed from all the oceans. Furthermore, the importance of organic Fe(II) complexes ought to be explored in the laboratory and in the ocean.

Our long-term goal is to understand the role of iron in ocean biogeochemical cycles. A comprehensive model of ocean biogeochemistry would include biological, chemical, physical, and radiative processes. Because iron chemistry influences the biological uptake of dissolved iron and sinking of particulate iron, the iron chemistry should be integrated into such a model to understand the biological impact of atmospheric deposition of soluble iron or anthropogenic iron fertilization and to study transport of iron from coastal to pelagic oceans. A validated biogeochemistry model of carbon and nutrients including iron in the ocean is a useful tool for the study of both natural and anthropogenic climate change and its coupling to carbon cycle and dust emissions.

Acknowledgment

I am deeply grateful to Francois Morel (Princeton University) for useful discussions, and to John Dunne (NOAA Geophysical Fluid Dynamics Laboratory), George Luther III (University of Delaware) and two

anonymous reviewers for their insightful comments and suggestions to revise the paper.

References

Arakaki, T., Fujimura, H., Hamdun, A.M., Okada, K., Kondo, H., Oomori, T., Tanahara, A., Taira, H., 2005. Simultaneous measurement of hydrogen peroxide and Fe species (Fe(II) and Fe(tot)) in Okinawa Island Seawater: impacts of red soil pollution. Journal of Oceanography 61, 561–568.

Armbrust, E.V., et al., 2004. The genome of the diatom *Thalassiosira Pseudonana*: ecology, evolution, and metabolism. Science 306, 79–86.

Armstrong, R.A., 1999. An optimization-based model of iron-light-ammonium colimitation of nitrate uptake and phytoplankton growth. Limnology and Oceanography 44 (6), 1436–1446.

Armstrong, E., Granger, J., Mann, E.L., Price, N.M., 2004. Outer-membrane siderophore receptors of heterotrophic oceanic bacteria. Limnology and Oceanography 49, 579–587.

Avery Jr., G.B., Cooper, W.J., Kieber, R.J., Willey, J.D., 2005. Hydrogen peroxide at the Bermuda Atlantic Time Series Station: temporal variability of seawater hydrogen peroxide. Marine Chemistry 97, 236–244.

Barbeau, K., 2006. Photochemistry of organic iron(III) complexing ligands in oceanic systems. Photochemistry and Photobiology 82, 1505–1516.

Barbeau, K., Moffett, J., 2000. Laboratory and field studies of colloidal iron oxide dissolution as mediated by phagotrophy and photolysis. Limnology and Oceanography 45, 827–835.

Barbeau, K., Moffett, J., Caron, D., Croot, O., Erdner, D., 1996. Role of protozoan grazing in relieving iron limitation of phytoplanlton. Nature 380, 61–64.

Barbeau, K., Rue, E., Bruland, K., Butler, A., 2001. Photochemical cycling of iron in the surface ocean mediated by microbial iron(III)-binding ligands. Nature 413, 409–413.

Barbeau, K., Rue, E., Trick, C., Bruland, K., Butler, A., 2003. Photochemical reactivity of siderophores produced by marine heterotrophic bacteria and cyanobacteria based on characteristic Fe(III) binding groups. Limnology and Oceanography 48, 1069–1078.

Berdnikov, V.M., 1973. Catalytic activity of the hydrated copper ion in the decomposition of hydrogen peroxide. Russian Journal of Physical Chemistry 47, 1060–1062.

Bergquist, B.A., Wu, J., Boyle, E.A., 2007. Variability in oceanic dissolved iron is dominated by the colloidal fraction. Geochimica et Cosmochimica Acta 71, 2960–2974.

Bielski, B.H.J., 1978. Reevaluation of the spectral and kinetic properties of HO_2 and O_2^- free radicals. Photochemistry and Photobiology 28, 645–649.

Bjergbakke, E., Sehested, K., Rasmussen, O.L., 1976. The reaction mechanism and rate constants in the radiolysis of Fe^{2+}/Cu^{2+} solutions. Radiation Research 66, 433–442.

Borer, P.M., Sulzberger, B., Reichard, P., Kraemer, S.M., 2005. Effect of siderophores on the light-induced dissolution of colloidal iron(III) (hydr)oxides. Marine Chemistry 93, 179–193.

Boyd, P.W., Crossley, A.C., DiTullio, G.R., Griffiths, F.B., Hutchins, D.A., Queguiner, B., Sedwick, P.N., Trull, T.W., 2001. Control of phytoplankton growth by iron supply and irradiance in the subantarctic Southern Ocean: Experimental results from the SAZ Project. Journal of Geophysical Research 106 (C12), 31,573–31,583.

Boyd, P.W., et al., 2005. FeCycle: attempting an iron biogeochemical budget from a mesoscale SF_6 tracer experiment in unperturbed low iron waters. Global Biogeochemical Cycles 19, GB4S20. doi:10.1029/2005GB002494.

Buck, K.N., Bruland, K.W., 2007. The photochemical speciation of dissolved iron in the Bering Sea, Alaska. Limnology and Oceanography 52 (5), 1800–1808.

Coale, K.H., Bruland, K.W., 1990. Spatial and temporal variability in copper complexation in the North Pacific. Deep-Sea Research 37, 317–336.

Cooper, W.J., Lean, D.R.S., Carey, J., 1989. Spatial and temporal patterns of hydrogen peroxide in lake waters. Canadian Journal of Fisheries and Aquatic Sciences 46, 1227–1231.

Croot, P.L., Laan, P., Nishioka, J., Strass, V., Cisewski, B., Boye, M., Timmermans, K.R., Bellerby, R.G., Goldson, L., Nightingale, P., de Baar, H.J.W., 2005. Spatial and temporal distribution of Fe(II) and H_2O_2 during EisenEx, and open ocean mescoscale iron enrichment. Marine Chemistry 95, 65–88.

Davey, M.S., Suggett, D.J., Geider, R.J., Taylor, A.R., 2003. Phytoplankton plasma membrane redox activity: Effect of iron limitation and interaction with photosynthesis. Journal of Phycology 39, 1132–1144.

DuRand, M.D., Olson, R.J., Chisholm, S.W., 2001. Phytoplankton population dynamics at the Bermuda Atlantic Time-series station in the Sargasso Sea. Deep-Sea Research. Part 2. Topical Studies in Oceanography 48, 1983–2003.

Emmenegger, L., Schonberger, R., Sigg, L., Sulzberger, B., 2001. Light-induced redox cycling of iron in circumneutral lakes. Limnology and Oceanography 46, 49–61.

Frouin, R., Lingner, D.W., Gautier, C., Baker, K.S., Smith, R.C., 1989. A simple analytical formula to compute clear sky total and photosynthetically available solar irradiance at the ocean surface. Journal of Geophysical Research 94 (C7), 9731–9742.

Fujii, M., Rose, A.L., Waite, T.D., Omura, T., 2006. Superoxide-mediated dissolution of amorphous ferric oxyhydroxide in seawater. Environmental Science and Technology 40, 880–887.

Gerringa, L.J.A., Rijkenberg, M.J.A., Timmermans, K.R., Buma, A.G.J., 2004. The influence of solar ultraviolet radiation on the photochemical production of H_2O_2 in the equatorial Atlantic Ocean. Journal of Sea Research 51, 3–10.

Hudson, R.J.M., Morel, F.M.M., 1990. Iron transport in marine phytoplankton: Kinetics of cellualar and medium coordination reactions. Limnology and Oceanography 35 (5), 1002–1120.

Hudson, R.J.M., Morel, F.M.M., 1993. Trace metal transport by marine microorganisms: Implications of metal coordination kinetics. Deep-Sea Research. Part 1. Oceanographic Research Papers 40 (1), 129–150.

Hutchins, D.A., DiTullio, G.R., Bruland, K.W., 1993. Iron and regenerated production: Evidence for biological iron recycling in two marine environments. Limnology and Oceanography 38 (6), 1242–1255.

Johnson, K., Coale, K., Elrod, V., Tindale, N., 1994. Iron photochemistry in seawater from the equatorial Pacific. Marine Chemistry 46, 319–334.

Johnson, K., et al., 2007. Developing standards for dissolved iron in seawater. EOS, Transactions, vol. 88(11). American Geophysical Union.

Kuma, K., Nakabayashi, S., Suzuki, Y., Kudo, I., Matsunaga, K., 1992. Photo-reduction of Fe(III) by dissolved organic substances and existence of Fe(II) in seawater during spring blooms. Marine Chemistry 37, 15–27.

Kuma, K., Nishioka, J., Matsunaga, K., 1996. Controls on iron(III) hydroxide solubility in seawater: The influence of pH and natural organic chelators. Limnology and Oceanography 41, 396–407.

Kustka, A.B., Shaked, Y., Milligan, A.J., King, D.W., Morel, F.M.M., 2005. Extracellular production of superoxide by marine diatoms:

Constrasting effects on iron redox chemistry and bioavailability. Limnology and Oceanography 50 (4), 1172–1180.
Laglera, L.M., van den Berg, C.M.G., 2006. Photochemical oxidation of thiols and copper complexing ligands in estuarine waters. Marine Chemistry 101 (1–2), 130–140.
Liu, X., Millero, F.J., 2002. The solubility of iron in seawater. Marine Chemistry 77, 43–54.
Lumb, F.E., 1964. The influence of cloud on hourly amount of total solar radiation at the sea surface. Quarterly Journal of the Royal Meteorological Society 90, 43–56.
Maldonado, M., Price, N.M., 1999. Utilization of iron bound to strong organic ligands by plankton communities in the subarctic North Pacific. Deep-Sea Research. Part 2. Topical Studies in Oceanography 46, 2447–2473.
Maldonado, M., Price, N.M., 2001. Reduction and transport of organically bound iron by *Thalassiosira oceanica* (Bacillariophycease). Journal of Phycology 37, 298–309.
Maldonado, M., Strzepek, R.F., Sander, S., Boyd, P.W., 2005. Acquisition of iron bound to strong organic compexes, with different Fe binding groups and photochemical reactivities, by phytoplankton communities in Fe-limited subantarctic waters. Global Biogeochemical Cycles 19, GB4S23. doi:10.1029/2005GB002481.
Mann, E.L., Ahlgren, A., Moffett, J.W., Chisholm, S.W., 2002. Copper toxicity and cyanobateria ecology in the Sargasso Sea. Limnology and Oceanography 47 (4), 976–988.
Marshall, J.-A., Hovenden, M., Oda, T., Hallegraeff, G.M., 2002. Photosynthesis does influence superoxide production in the ichthyotoxic alga *Chattonella marina* (Raphidophyceae). Journal of Plankton Research 24 (11), 1231–1236.
Marshall, J.-A., de Salas, M., Oda, T., Hallegraeff, G., 2005. Superoxide production by marine microalgae, I. Survey of 37 species from 6 classes. Marine Biology 147, 533–540.
Martin, J., 1990. Glacial–interglacial CO_2 change: the iron hypothesis. Paleooceanography 5, 1–13.
Meunier, L., Laubscher, H., Hug, S.J., Sulzberger, B., 2005. Effects of size and origin of natural dissolved organic matter compounds on the redox cycling of iron in sunlit surface waters. Aquatic Sciences 67, 292–307.
Micinski, E., Ball, L.A., Zafiriou, O.C., 1993. Photochemical oxygen activation: Superoxide radical detection and production rates in the Eastern Caribbean. Journal of Geophysical Research 98 (C2), 2299–2306.
Miller, W.L., King, D.W., Lin, J., Kester, D.R., 1995. Photochemical redox cycling of iron in coastal seawater. Marine Chemistry 50, 63–77.
Millero, F., Sotolongo, S., 1989. The oxidation of Fe(II) with H_2O_2 in seawater. Geochimica et Cosmochemica Acta 53, 1867–1873.
Millero, F., Sotolongo, S., Izaguirre, M., 1987. The oxidation kinetics of Fe(II) in seawater. Geochimica et Cosmochemica Acta 51, 793–801.
Moffet, J.W., 1995. Temporal and spatial variability of strong copper complexing ligands in the Sargasso Sea. Deep-Sea Research. Part 1. Oceanographic Research Papers 42 (8), 1273–1295.
Moffet, J.W., Dupont, C., 2007. Cu complexation by organic ligands in the sub-arctic NW Pacific and Bering Sea. Deep-Sea Research. Part 1. Oceanographic Research Papers 54 (4), 586–595.
Moffet, J.W., Zafiriou, O.C., 1990. An investigation of hydrogen peroxide chemistry in surface waters of Vineyard Sound with $H_2^{18}O_2$ and $^{18}O_2$. Limnology and Oceanography 35 (6), 1221–1229.
Moore, C.A., Farmer, C.T., Zika, R.G., 1993. Influence of the Orinoco River on hydrogen peroxide distribution and production in the Eastern Caribbean. Journal of Geophysical Research 98 (C2), 2289–2298.
Mopper, K., Zhou, X., 1990. Hydroxyl radical photoproduction in the sea and its potential impact on marine processes. Science 250, 661–664.
Morel, F.M.M., Price, N.M., 2003. The biogeochemical cycles of trace metals in the oceans. Science 300, 944–947.
Nelson, N.B., Siegel, D.A., Michaels, A.F., 1998. Seasonal dynamics of colored dissolved material in the Sargasso Sea. Deep-Sea Research. Part 1. Oceanographic Research Papers 45, 931–957.
Nelson, N.B., Carlson, C.A., Steinberg, D.K., 2004. Production of chromophoric dissolved organic matter by Sargasso Sea microbes. Marine Chemistry 89, 273–287.
Nishioka, J., Takeda, S., Wong, C.S., Johnson, K.W., 2001. Size-fractionated iron concentrations in the northeast Pacific Ocean: distribution of soluble and small colloidal iron. Marine Chemistry 74, 157–179.
Nishioka, J., Takeda, S., Kudo, I., Tsumune, D., Yoshimura, T., Kuma, K., Tsuda, A., 2003. Size-fractionated iron distributions and iron-limitation processes in the subarctic NW Pacific. Geophysical Research Letters 30 (14), 1730. doi:10.1029/2002GL016853.
Palenik, B., Morel, F.M.M., 1988. Dark production of H_2O_2 in the Sargasso Sea. Limnology and Oceanography 33 (6, part 2), 1601–1611.
Palenik, B., Zafiriou, O.C., Morel, F.M.M., 1987. Hydrogen peroxide production by a marine phytoplankter. Limnology and Oceanography 32 (6), 1365–1369.
Petasne, R.G., Zika, R.G., 1987. Fate of superoxide in coastal sea water. Nature 325, 516–518.
Piechowski von, Nauser, M.T., Hoigne, T., Buhler, R.E., 1993. O_2^- decay catalysed by Cu^{2+} and Cu^+ ions in aqueous solutions: a pulse radiolysis study of atmospheric chemistry. Berichte der Bunsengesellschaft fuÉr Physikalische Chemie 97, 762–771.
Rabani, J., Klug-Roth, D., Lilie, J., 1973. Pulse radiolytic investigations of the catalyst diproportionation of peroxy radicals, Aqueous cupric ions. Journal of Physical Chemistry 77, 1169–1173.
Rijkenberg, M.J.A., Fischer, A.C., Kroon, J.J., Gerringa, L.J.A., Timmermans, K.R., Wolterbeek, H.T., de Baar, H.J.W., 2005. The influence of UV irradiation on the photoreduction of iron in the Southern Ocean. Marine Chemistry 93, 119–129.
Rijkenberg, M.J.A., Gerringa, L.J.A., Carolus, V.E., Velzeboer, I., de Baar, H.J.W., 2006. Enhancement and inhibition of iron photoreduction by individual ligands in open ocean seawater. Geochimica et Cosmochimica Acta 70, 2790–2805.
Rose, A.L., Waite, T.D., 2003a. Predicting iron speciation in coastal waters from kinetics of sunlight-mediated iron redox cycling. Aquatic Sciences 65, 375–383.
Rose, A.L., Waite, T.D., 2003b. Kinetics of iron complexation by dissolved natural organic matter in coastal waters. Marine Chemistry 84, 85–103.
Rose, A.L., Waite, T.D., 2005. Reduction of organically complexed ferric iron in seawater. Environmental Science and Technology 39, 2645–2650.
Roy, E.G., Wells, M.L., King, D.W., 2008. Persistence of iron(II) in surface waters of the western subarctic Pacific. Limnology and Oceanography 53 (1), 89–98.
Rue, E.L., Bruland, K.W., 1995. Complexation of iron(III) by natural organic ligands in the Central North Pacific as determined by a new competitive ligand equilibration/adsorptive cathodic stripping voltammetric method. Marine Chemistry 50, 117–138.
Rush, J.D., Bielski, B.H.J., 1985. Pulse radiolytic studies of the reactions of HO_2/O_2^- with Fe(II)/Fe(III) ions. The reactivity of HO_2/O_2^- with ferric ions and its implication on the occurrence of the Haber–Weiss reaction. Journal of Physical Chemistry 89, 5062–5066.

Sedwick, P.N., Church, T.M., Bowie, A.R., Marsay, C.M., Ussher, S.J., Achilles, K.M., Lethaby, P.J., Johnson, R.J., Sarin, M.M., McGillicuddy, D.J., 2005. Iron in the Sargasso Sea (Bermuda Atlantic Time-series Study region) during summer: Eolian imprint, spatiotemporal variability, and ecological implications. Global Biogeochemical Cycles 19, GB4006. doi:10.1029/2004GB002445.

Shaked, Y., Kustka, A.D., Morel, F.M.M., 2005. A general kinetic model for iron acquisition by eukaryotic phytoplankton. Limnology and Oceanography 50 (3), 872–882.

Stinzi, A., Barnes, C., Xu, J., Raymond, K.N., 2000. Microbial iron transport via a sideriophore shuttle: a membrane ion transport paradigm. Proceedings of the National Academy of Sciences, vol. 97, pp. 10691–10696.

Sulzberger, B., Laubscher, H.U., 1995. Reactivity of various types of iron(III) (hydr)oxides towards light-induced dissolution. Marine Chemistry 50, 103–115.

Sunda, W., Huntsman, S., 1995. Iron uptake and growth limitation in oceanic and coastal phytoplankton. Marine Chemistry 50, 189–206.

Tagliabue, A., Arrigo, K.R., 2006. Processes governing the supply of iron to phytoplankton in stratified seas. Journal of Geophysical Research 111, C06019. doi:10.1029/2005JC003363.

Takata, H., Kuma, K., Saitoh, Y., Chikira, M., Saitoh, S., Isoda, Y., Takagi, S., Sakaoka, K., 2006. Comparing the vertical distribution of iron in the eastern and western North Pacific Ocean. Geophysical Research Letters 33, L02613. doi:10.1029/2005GL024538.

Vodacek, A., Blough, N.V., DeGrandpre, M.D., Peltzer, E.T., Nelson, R.K., 1997. Seasonal variation of CDOM and DOC in the Middle Atlantic Bight: Terrestrial inputs and photooxidation. Limnology and Oceanography 42 (4), 674–686.

Voelker, B.M., Morel, F.M.M., Sulzberger, B., 1997. Iron redox cycling in surface waters: effects of humic substances and light. Environmental Science and Technology 31, 1004–1011.

Waite, T.D., Morel, F.M.M., 1984. Photoreductive dissociation of colloidal iron oxides in natural waters. Environmental Science and Technology 18, 860–868.

Weber, L., Volker, C., Schartau, M., Wolf-Gladrow, D.A., 2005. Modeling the speciation and biogeochemistry of iron at the Bermuda Atlantic Time-series Study site. Global Biogeochemical Cycles 19, GB1019. doi:10.1029/2004GB002340.

Wells, M.L., Mayer, L.M., 1991. The photoconversion of colloidal iron oxyhydroxides in seawater. Deep-Sea Research 38, 1379–1395.

Wells, M.L., Trick, C.G., 2004. Controlling iron availability to phytoplankton in iron-replete coastal waters. Marine Chemistry 86, 1–13.

Wells, M.L., Mayer, L.M., Donard, O.F.X., de Souza Sierra, M.M., Ackelson, S.G., 1991. The photolysis of colloidal iron in the oceans. Nature 353, 248–250.

Witter, A., Luther III, G., 1998. Variation of Fe-organic complexation with depth in the northwestern Atlantic Ocean as determined using a kinetic approach. Marine Chemistry 62, 241–258.

Witter, A., Hutchins, D., Butler, A., Luther III, G., 2000. Determination of conditional stability constants and kinetic constants for strong model Fe-binding ligands in seawater. Marine Chemistry 69, 1–17.

Wu, J., Luther III, G.W., 1995. Complexation of Fe(III) by natural organic ligands in the Northwest Atlantic Ocean by a competitive ligand equilibration method and a kinetic approach. Marine Chemistry 50, 159–178.

Wu, J., Boyle, E., Sunda, W., Wen, L., 2001. Soluble and colloidal iron in the oligotrophic North Atlantic and North Pacific. Science 293, 847–849.

Yuan, J., Shiller, A.M., 2001. The distribution of hydrogen peroxide in the southern and central Atlantic Ocean. Deep-Sea Research. Part 2. Topical Studies in Oceanography 48, 2947–2970.

Yuan, J., Shiller, A.M., 2005. Distribution of hydrogen peroxide in the northwest Pacific Ocean. Geochemistry, Geophysics, Geosystems 6 (9), Q09M02. doi:10.1029/2004GC000908.